JOURNAL OF PROPULSION AND POWER
Vol. 12, No. 4, July–August 1996

Injection of Supercritical Ethylene in Nitrogen

Pei-Kuan Wu* and Tzong H. Chen†
Taitech, Inc., Beavercreek, Ohio 45440
Abdollah S. Nejad‡
U.S. Air Force Wright Laboratory, Wright–Patterson AFB, Ohio 45433
and
Campbell D. Carter§
Systems Research Laboratories, Inc., Dayton, Ohio 45440

The injection of supercritical fuel into a quiescent gas environment was experimentally studied to elucidate the effects of thermophysical and transport properties near the critical point on jet appearance, shock structures, and choking. Ethylene and nitrogen were used to simulate interactions between fuel and air. Conditions near the thermodynamic critical point of ethylene are considered, with supercritical temperatures and pressures upstream of the injector and subcritical pressures downstream of the injector. Flow visualization showed an opaque region resulting from fuel condensation when fuel was injected at near room temperature. At higher injectant temperatures, the ethylene jet was found to have a shock structure similar to that of an underexpanded ideal-gas jet. Mass flow rates were found to be insensitive to the variation of back pressure, indicating that the jet flow is choked. Mass flow rates were normalized by those values calculated for ideal-gas jets under the same conditions. The normalized mass flow rate first increases as injection conditions approach the critical temperature, apparently because of the rapid increase in fluid density, and then decreases, possibly as a result of the coexistence of liquid and gas phases at the nozzle exit.

Nomenclature

A = cross-sectional area
a = speed of sound
d = nozzle exit diameter
h = fluid enthalpy
M = Mach number
$\mathcal{M}$ = gas molecular weight
$\dot{m}$ = fuel mass flow rate
P = pressure
R = universal gas constant
Re = Reynolds number based on nozzle diameter, $\rho du/\mu$
T = temperature
u = fluid velocity
γ = gas specific heat ratio, C_p/C_v
μ = fluid viscosity
ρ = fluid density

Subscripts
chm = gas property in injection chamber
e = nozzle exit condition
ideal = calculated property based on ideal-gas, isentropic-flow assumption
inj = injectant property before reaching nozzle passage
r = reduced property, normalized by its critical value

Superscript
* = choked condition

Received June 14, 1995; revision received Dec. 18, 1995; accepted for publication Jan. 4, 1996.

*Research Scientist, 3675 Harmeling Drive. Member AIAA.
†Chief Scientist. Senior Member AIAA.
‡Senior Research Scientist, Aero Propulsion and Power Directorate.
§Research Scientist, 2800 Indian Ripple Road. Member AIAA.

Introduction

FOR hypersonic flight, e.g., flight Mach numbers greater than 8, thermal management of the airframe and of onboard electronic components is an engineering challenge.[1] Conventional cooling techniques using ambient air are not feasible at hypersonic speeds because the stagnation temperature of the air is higher than the high-temperature limit of current aerospace materials. One solution to this problem would be regenerative fuel cooling of the airframe and the combustor components. Endothermic fuels are being investigated as candidates for this type of application.[1] An endothermic fuel is one that can undergo an endothermic thermal cracking (pyrolysis) reaction with a very large reaction heat. It has been shown that the thermal cracking reaction of endothermic fuels occurs at very high temperatures; *n*-dodecane, for example, is stable to 1100 K, before thermal cracking becomes significant. These reaction temperatures are generally much higher than the critical temperature of hydrocarbon fuels, e.g., the critical temperature for *n*-dodecane is 659 K, and the heat management of future aircraft is expected to require the use of supercritical fuels.[1]

The combustor operating conditions are vastly different for the missile's startup, boost, cruise, and final approach phases, and since fuel is used to absorb heat from the combustor for all phases, broad ranges of fuel operating temperatures and pressures are encountered. Thus, the regenerative fuel cooling approach increases the complexity of the fuel system and strongly affects injection and mixing mechanisms. Fuel may be injected as liquid under subcritical conditions or as gas under supercritical conditions, depending on the extent of heating and the fuel's thermodynamic states at the nozzle exit. Furthermore, supercritical fuels exhibit unusual thermophysical and transport properties near their critical point: liquid-like density, zero latent heat, zero surface tension, and low compressibility. These fuels also exhibit large variations in specific heats and speeds of sound, and enhanced values of thermal conductivity, viscosity, and mass diffusivity.[2–4]

An ethylene phase diagram of fluid density as a function of pressure is shown in Fig. 1; the diagram is based on the ther-

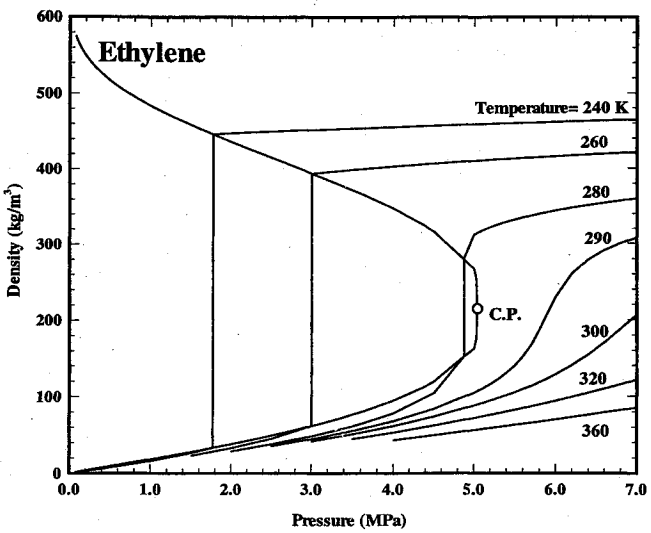

Fig. 1 ρ–P–T diagram for ethylene.

modynamic properties reported by Younglove.[4] Selected isotherms are plotted to illustrate the density variation; C.P. denotes the thermodynamic critical point. Note that the gradient of fluid density with respect to temperature and pressure is extremely large near the critical point. Thus, for an isothermal process starting at the critical point, a 10% decrease in fluid pressure results in a decrease in fluid density of more than 50%. This is a clear illustration of how the injection characteristics of a fuel under conditions near its critical point can be dramatically different from those of liquids[5,6] or ideal gases.[7,8]

Previous studies of supercritical fuel injection and atomization processes have been limited in scope and have focused primarily on processes at temperatures lower than the critical temperature of the fuel.[9,10] Chen[9] studied the atomization processes of sulfur hexafluoride (SF_6) injected at near critical temperatures into quiescent gaseous environments and found that spray penetration decreases as fuel temperature increases. This decrease is related to the decrease of the density of the fuel as it enters the supercritical state. Hermanson et al.[10] studied the injection of cryogenic nitrogen near the critical temperature into a supersonic crossflow. They found a reduction in penetration height, compared to that observed for the injection of subcritical ethanol, which they attributed to a larger degree of superheat. Yang et al.[11] studied liquid-fuel droplet combustion in both subcritical and supercritical environments and suggested that the combustion mechanism changed considerably at the critical pressure, mainly as a result of reduced mass diffusivity and latent heat of vaporization with increased pressure. These studies indicate that the atomization, mixing, and burning processes of supercritical fluids are significantly different from those observed under subcritical conditions. However, no study has been conducted on the injection of supercritical fluids under conditions near and above the thermodynamic critical point.

The objective of the present investigation was to study the injection of a supercritical fuel at injection temperatures slightly greater than the fuel's critical temperature, with back pressures lower than the critical pressure. Therefore, the injection of ethylene starts the injection process under supercritical conditions and is superheated by the end of the process. Test conditions were designed to simulate injection of an endothermic fuel at temperatures between the critical temperature and the point where thermal cracking becomes significant. For n-dodecane, one of the endothermic fuels currently being tested, this temperature range comprises a range of reduced temperatures T_r, defined as temperature normalized by its critical value, of 1.0–1.67.[1] Therefore, in this study ethylene is injected with T_r, from 1.04 to 1.29, into quiescent nitrogen. For ideal gases with large enough variations of pressure, an underexpanded jet is obtained; this process has been well characterized.[7,8] The experimental results of the present study were compared with those from ideal-gas studies to illustrate the effects of near-critical-point thermophysical and transport properties on jet appearance and near-field shock structures. This article begins with a description of the experimental methods, followed by the results of a system validation using nitrogen as the injectant. Results for ethylene injection into ambient nitrogen are then discussed, treating flow visualization, mass flow rate measurements, and thermodynamic path analysis during injection. Finally, the differences between the injection processes of a supercritical fuel and an ideal gas are discussed.

Experimental Methods

Apparatus

The test fluid was injected vertically downward into a large injection chamber filled with an inert gas (nitrogen) to study the effects of fuel temperature and ambient back pressure on jet structure and mass flow rate for a fuel near its critical temperature. The apparatus consists of a fuel tank, a solenoid valve, a fuel temperature control unit, a nozzle, and the injection chamber (Fig. 2).

The fuel tank assembly was designed to allow preset initial fuel pressures and temperatures and to provide a steady fuel supply during injection. The fuel tank was a commercial ethylene bottle with an internal volume of 43.5 l. The large volume was necessary to minimize variations of injectant pressure during injection. Injection pressures were controlled to within ±1% of the preset values for all present test conditions. The ethylene bottle and fuel tank were wrapped with copper tubes through which water at 313 K was circulated to prevent fuel condensation and to provide a constant initial fuel temperature. A solenoid valve with a response time of 150 ms was installed in the fuel delivery line to control the injection duration. Injection times were limited to 5–8 s to minimize fuel consumption and to maximize the number of test runs before a significant fuel vapor partial pressure was reached in the injection chamber.

Supercritical fuel temperatures were monitored with thermocouples and controlled by flowing ethylene glycol outside the fuel pipe along the fuel delivery line for a distance of over 6 m upstream of the nozzle. Through the use of a heat exchanger, the temperature of the ethylene glycol was maintained between 293–422 K, with an uncertainty of ±1 K. Tests

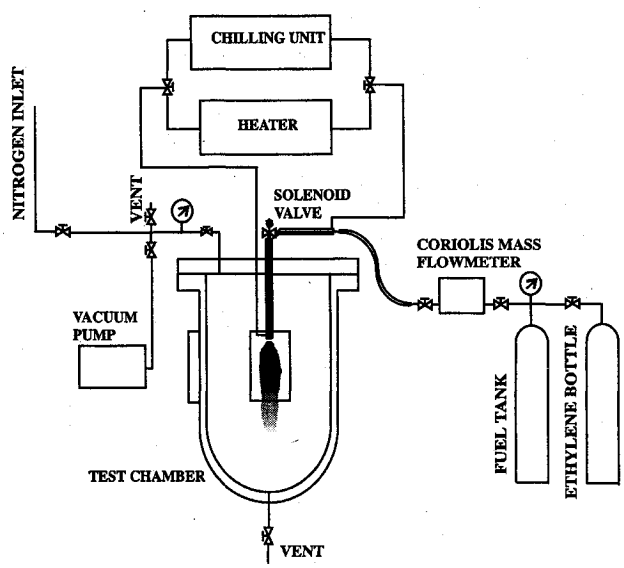

Fig. 2 Sketch of supercritical fuel injection apparatus.

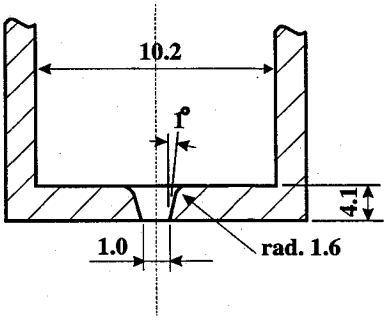

Fig. 3 Sketch of the nozzle passage; lengths are in mm.

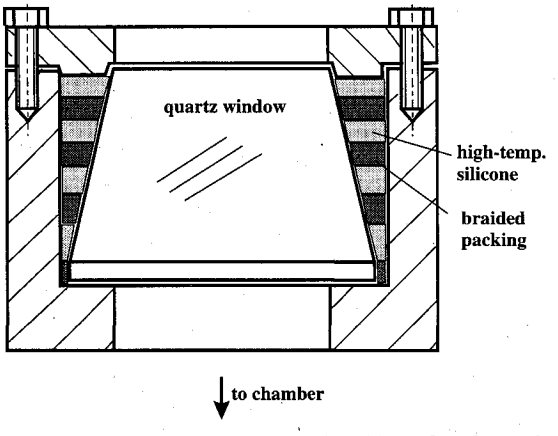

Fig. 4 Schematic diagram of the injection chamber window design.

showed that the final fuel temperature was within 2 K of the coolant temperature for moderate temperatures; the fuel temperatures reported in this study are the coolant temperatures. For higher temperatures, larger uncertainties would be expected (4 K), because of the limited heating capacity of the current heater arrangement. The fuel static pressure was measured upstream of the nozzle passage with a bridge-type pressure transducer having an uncertainty within ±7 kPa. The measured fuel static pressure was used as the fuel stagnation pressure (injection pressure) in the following discussion, since the fluid velocities in the fuel delivery line were negligible. The measured pressure and temperature were then used to quantify the fuel properties before injection.

The nozzle passage consisted of a rounded entry and a converging section, as shown in Fig. 3. The entry, with a radius of 1.6 mm, was followed by a 1-deg converging passage to ensure that a choked point could occur only at the nozzle exit. The nozzle exit diameter was 1 mm, and the ratio of passage length to exit diameter was selected to be 4. This arrangement yielded a cross-sectional area ratio of the fuel delivery line to the nozzle exit passage of 104; this design minimizes the effect of upstream flow disturbances.[12]

To study the effects of ambient back pressure on the injection process, the fuel jet was enclosed in a large injection chamber. This chamber was designed to provide a high-pressure and temperature environment for the simulation of scramjet and gas turbine combustor conditions and industrial injector atomization processes. The chamber diameter is 0.42 m and its height is 0.94 m, resulting in an internal volume of 0.12 m^3. Four optical ports are provided for flow diagnostics. Two 63.5-mm-thick rectangular quartz windows, each having a clear aperture of 89 × 127 mm, were installed on opposite sides of the chamber. These windows were supported from the back by layers of high-temperature silicone and graphite braided packing to ensure sealing at high chamber pressures and temperatures (Fig. 4). A rupture disc set for 9.4 MPa and a relief valve set for 6.8 MPa were attached to the chamber for safety purposes. The chamber pressure was monitored by a second bridge-type pressure transducer, also having an uncertainty within ±7 kPa. The chamber, with the windows installed, was hydrostatically tested to 7 MPa at room temperature.

Before measurements were made, the chamber was flushed with nitrogen to remove oxygen. The fuel pressure and temperature were set by charging the fuel tank to a specified pressure and adjusting the temperature controller of the fuel heat exchanger. Measurements were begun by activating the solenoid valve; fuel and chamber pressures and temperatures were then recorded by a high-speed data-acquisition board linked to a 486 personal computer. During each run, the rise in chamber pressure was typically less than 34 kPa. After each run, the chamber was vented and reset to the desired pressure.

Instrumentation

Long-exposure shadowgraphs were used to identify the thermodynamic phase (i.e., gas or liquid) of the injectant. A 35-mm Nikon camera with a shutter speed of 1/30 s and an f-number of 4.5 was used to capture the shadowgraphs. The magnification selected was about 1.63 to permit visualization of the entire jet field. Schlieren photographs were employed to resolve shock patterns and jet boundaries. The schlieren system used a Speed Graphic camera, loaded with a Polaroid type 57, 100 × 125 mm black and white film with a shutter speed of 1/125 s. Two 300-mm-diam parabolic mirrors, with focal lengths of 1220 mm, collimated and focused the light from a mercury lamp. The arrangement provided an image magnification of 4.15 and a 22 mm^2 field of view (FOV).

The fuel mass flow rate was measured by a Coriolis-type mass flow meter (Fig. 2). This flow meter is designed for direct measurement of the mass flow rate of any fluid at a stable thermodynamic state, with an uncertainty of less than ±1%. However, the time response for this device is slow (approximately 4 s). During the present study, an injection duration of 8 s was normally employed, and mass flow rates were averaged for the last 4 s to obtain the mean mass flow rate for each run. Mass flow rates were averaged over five runs, yielding standard deviations of less than ±1%.

Test Conditions

The fuel temperature and pressure were set to be slightly above the critical point to study the effect of near-critical-point thermophysical properties on the injection process. Ethylene was chosen as a test fuel because its critical temperature is near room temperature, which reduces system safety requirements. Nitrogen was used as the ambient gas because it is inert and has properties similar to air. The test conditions are summarized in Table 1. Fuel pressures and temperatures are expressed as reduced values (i.e., relative to the critical point values of 5.04 MPa and 283 K). The fuel injection pressure was set between 5.7–5.8 MPa, ±1%, yielding reduced injection pressures from 1.13 to 1.15. Fuel temperatures were varied from 293 to 365 K, resulting in reduced temperatures from 1.04 to 1.29. Chamber pressures of 0.10–3.4 MPa provided ratios to the injection pressure (P_{chm}/P_{inj}) of 0.018–0.59, which results in sonic and subsonic flows when nitrogen is the injectant. Jet Reynolds numbers at the nozzle exit were estimated to be between 1.03–1.38 × 10^6 (see Table 2), based on the thermophysical properties of Younglove,[4] fluid viscosities from

Table 1 Summary of test conditions

Parameters	Ranges
P_{inj}/P_c [a]	1.13–1.15
T_{inj}/T_c [b]	1.04–1.29
P_{chm}/P_{inj}	0.018–0.59
T_{chm}/T_c	1.04

[a] P_c = 5.04 MPa. [b] T_c = 283 K.

Holland et al.,[3] and the isentropic approximation (discussed next).

Results and Discussion

Injection of Nitrogen

Nitrogen was injected into nitrogen to validate the experimental system. Because nitrogen is an ideal gas under the test conditions, its injection process is well understood.[8,13] These tests, therefore, provided a means of assessing the overall system accuracy as well as estimating the discharge coefficient of the nozzle passage. Assuming the process to be one dimensional and isentropic and the fluid to be an ideal gas with constant specific heats, the mass flow rate $\dot{m}$ through a circular cross-sectional nozzle (with an exit area A_e) can be expressed as follows:

$$\dot{m} = \sqrt{2\gamma/(\gamma-1)}\sqrt{(P_{chm}/P_{inj})^{(\gamma+1)/\gamma}[(P_{chm}/P_{inj})^{-(\gamma-1)/\gamma} - 1]} \times P_{inj}A_e/\sqrt{RT_{inj}/\mathcal{M}} \quad (1)$$

When an ideal gas undergoes an isentropic process with constant γ, the ratio of injection pressure to nozzle exit pressure is a function of M:

$$P_{inj}/P_e = [1 + (\gamma - 1)M^2/2]^{\gamma/(\gamma-1)} \quad (2)$$

The maximum value of (P_{inj}/P_e) for a convergent nozzle occurs when a sonic speed is reached at the nozzle exit ($M = 1$). Further decreases of the chamber pressure do not alter the nozzle exit condition; i.e., (P_{inj}/P_e) is a constant, but the nozzle exit pressure no longer equals the chamber pressure. For nitrogen, γ is equal to 1.50 under the injection conditions, and the choking pressure ratio $(P_{chm}/P_{inj})^*$ is 0.512 from Eq. (2). The $\dot{m}^*$ can be calculated by substituting $(P_{chm}/P_{inj})^*$ into Eq. (1). The mass flow rate of a subsonic jet relative to that of a choked jet can then be written as

$$\dot{m}/\dot{m}^* = \sqrt{(P_{chm}/P_{inj})^{(\gamma+1)/\gamma}[(P_{chm}/P_{inj})^{-(\gamma-1)/\gamma} - 1]} / \sqrt{[(\gamma+1)/2]^{-(\gamma+1)/(\gamma-1)}(\gamma-1)/2} \quad (3)$$

For a sonic jet, $\dot{m}/\dot{m}^*$ should be unity. The measured mass flow rates for nitrogen jets at different P_{chm}/P_{inj} were normalized by $\dot{m}^*$, using $\gamma = 1.50$. The normalized mass flow rates are plotted in Fig. 5, together with the calculated results from Eq. (3). A discharge coefficient of 0.97 for choked conditions and 1.03 for unchoked conditions is indicated. The agreement between experimental results and predictions is reasonable, considering the mass flow rate measurement uncertainty (1%) and the uncertainty of mass flow rate predictions from Eq. (3) (3.8%), because of uncertainties of pressure measurements and specific heat ratios. Therefore, the discharge coefficients differ from unity within experimental uncertainties. A near-unity discharge coefficient is expected based on values reported for nozzles with similar geometries.[14,15]

Figure 6 shows a schlieren photograph of nitrogen injected at 5.8 MPa and 293 K into nitrogen at atmospheric pressure and 293 K. The jet is highly underexpanded and produces a Mach disk at a distance of about 4.3 nozzle diameters downstream of the nozzle exit, in agreement with the prediction of 4.26 from the empirical correlation of Crist et al.[8] The shock structure, Mach disk, intercepting shock, and reflected shock appear clearly in the photograph. These structures will be used as a basis for comparison with the injection patterns of supercritical fuel in the following discussion.

Flow Visualization of Ethylene Jets

Shadowgraphy

Typical shadowgraphs of ethylene jets injected at 5.7 MPa and 293 K into nitrogen at chamber pressures of 0.14, 0.41, 1.36, and 3.4 MPa (resulting in P_{chm}/P_{inj} of 0.024–0.59) are illustrated in Fig. 7. Each jet undergoes a sudden expansion and produces a dome-shaped jet boundary at the nozzle exit to accommodate the large pressure drop. This dome-shaped jet boundary becomes less significant when the chamber pressure is increased, and the jet exhibits a straight surface at the nozzle exit when the chamber pressure is 3.40 MPa ($P_{chm}/P_{inj} = 0.59$). These phenomena agree qualitatively with the transition of an ideal gas from an underexpanded sonic jet to a subsonic jet. The dome-shaped jet boundary near the nozzle exit suggests the presence of shock structures similar to those in a highly underexpanded ideal-gas jet. However, further evidence is needed to confirm this behavior and to resolve the shock structures.

The ethylene jets studied here produce strong fuel condensation and exhibit an opaque region. The opaque region exists even when the fuel injection pressure is below the critical pressure. This region gradually disappears when the condensed fuel absorbs sufficient heat from the ambient nitrogen and returns to the gas state. At the lowest P_{chm}, 0.14 MPa, the expansion is dramatic and fuel condensation is moderate. As the chamber pressure is increased to 0.41 MPa, the jet expansion is substantially less than that with $P_{chm} = 0.14$ MPa; however, the jet exhibits a much darker and longer opaque region that extends beyond the FOV, about 43 nozzle diameters. Fuel condensation on this scale can potentially absorb a large amount of heat, and, therefore, delay chemical reactions and reduce the performance of a supersonic combustor. As the chamber pressure is increased further, however, the opaque region be-

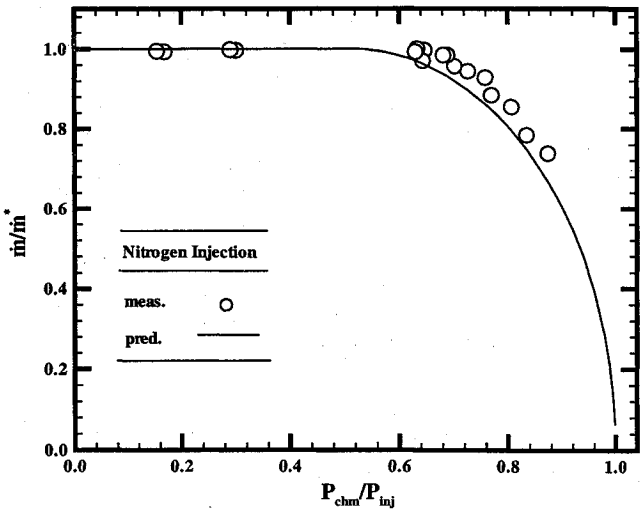

Fig. 5 Mass flow rates of nitrogen jets; $\dot{m}^*$ is based on $\gamma = 1.50$.

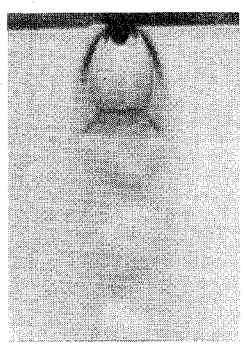

P_{inj}=5.8 MPa
P_{chm}=0.14 MPa
T_{inj}=293 K

Fig. 6 Schlieren photograph of an underexpanded nitrogen jet.

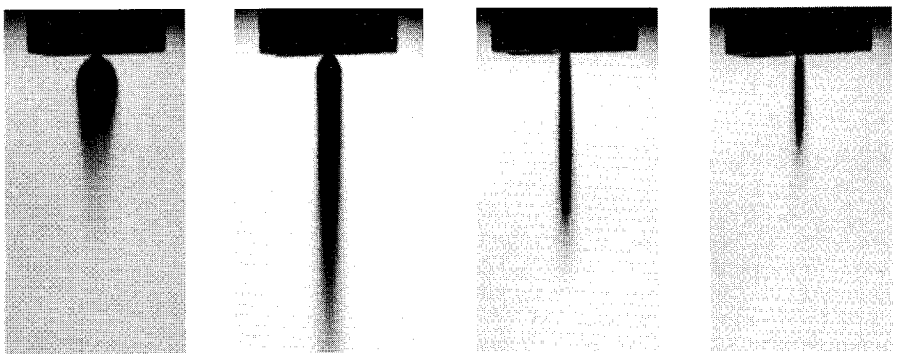

P_{inj}=5.7 MPa, P_{chm}=0.14 MPa, T_{inj}=293 K | P_{inj}=5.7 MPa, P_{chm}=0.41 MPa, T_{inj}=293 K | P_{inj}=5.7 MPa, P_{chm}=1.36 MPa, T_{inj}=293 K | P_{inj}=5.7 MPa, P_{chm}=3.40 MPa, T_{inj}=293 K

Fig. 7 Shadowgraphs of ethylene jets injected at 293 K into various chamber pressures.

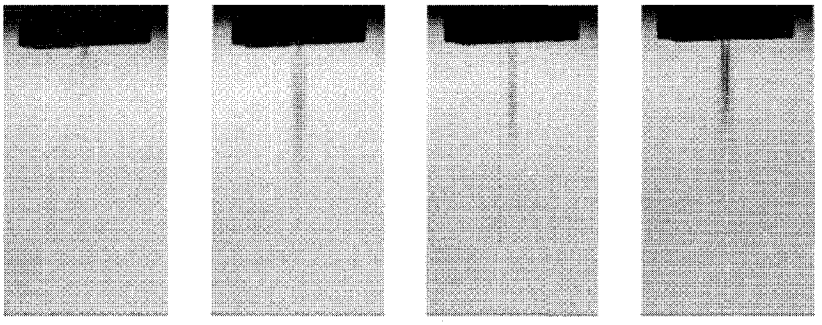

P_{inj}=5.7 MPa, P_{chm}=0.14 MPa, T_{inj}=325 K | P_{inj}=5.7 MPa, P_{chm}=0.41 MPa, T_{inj}=325 K | P_{inj}=5.7 MPa, P_{chm}=1.36 MPa, T_{inj}=325 K | P_{inj}=5.7 MPa, P_{chm}=3.40 MPa, T_{inj}=325 K

Fig. 8 Shadowgraphs of ethylene jets injected at 325 K into various chamber pressures.

comes shorter. Further studies are needed to characterize the fuel condensation phenomenon.

At higher injection temperatures, fuel condensation becomes less significant. Figure 8 shows shadowgraphs of typical ethylene jets injected at 5.7 MPa and 325 K into nitrogen at various chamber pressures. Note that only T_{inj} has been changed from the configuration discussed previously; P_{inj} remains the same. The ethylene jets still show condensation at this injection temperature, although the opaque region is smaller and not as dark as with T_{inj} = 293 K. The qualitative trend of fuel condensation with respect to chamber pressures remains similar, and as at the lower T_{inj}, the dome-shaped expansion is still visible at lower P_{chm}. Shock structures can now be identified at the nozzle exit, indicating that the jet is sonic exiting the nozzle. Mach disk locations were found to be 4.3 and 2.5 nozzle diameters downstream of the nozzle exit for chamber pressures of 0.14 and 0.41 MPa, respectively. The correlation of Crist et al.[8] predicts 4.1 and 2.4 nozzle diameters downstream as the location of Mach disks under these conditions. The correlation of Crist et al.[8] describes the injection process of a nondiffusing homogeneous substance (e.g., nitrogen injection into nitrogen). However, effects of nonhomogeneity (ethylene and nitrogen) are expected to be negligible for the conditions of the present study because of the small flow residence times for supersonic flows in the shock plume and much lower chamber pressures than the ethylene critical pressure; this argument is supported by the good agreement between the predictions of Crist et al.[8] and the present experimental observations. Furthermore, the agreement suggests that the injection of supercritical fuel under the test conditions listed in Fig. 8 produces results that are similar, at least in some respects, to those of an ideal gas. No measurement of Mach disk locations can be made at lower injection temperatures because of excessive fuel condensation. At higher injection temperatures, on the other hand, fuel condensation is so weak that shadowgraphy fails to record the jet image. Therefore, schlieren photography was employed to resolve the shock structures near the nozzle exit.

Schlieren Photography

Figure 9 shows schlieren photographs of ethylene injected at various temperatures (293, 325, 338, and 365 K) into nitrogen at 0.14 MPa and 293 K. The jets undergo a sudden expansion after leaving the nozzle. At lower temperatures, the ethylene jet exhibits an opaque region near the nozzle exit. As the injection temperature increases, the opaque region becomes lighter, and at T_{inj} = 338 K the Mach disk and intercepting and reflected shocks become evident. This indicates that increases in temperature shift the thermodynamic path and, as a consequence, the fuel does not pass through the liquid–gas mixture regime.

As mentioned in reference to Fig. 8, ethylene jets at conditions of higher T_{inj} are similar in appearance to nitrogen jets. It can, therefore, be argued that an ethylene jet at higher T_{inj} is thermodynamically farther away from its critical point than a jet at lower T_{inj} and should behave more like an ideal gas. The Mach disk locations for jets at T_{inj} = 338 and 365 K are about 4.1 and 3.9 mm, respectively, in close agreement to the value of 4.2 mm predicted by Crist et al.[8] Furthermore, Crist et al. found that the Mach disk location was a function of P_{chm}/P_{inj} alone, which agrees with the present observation.

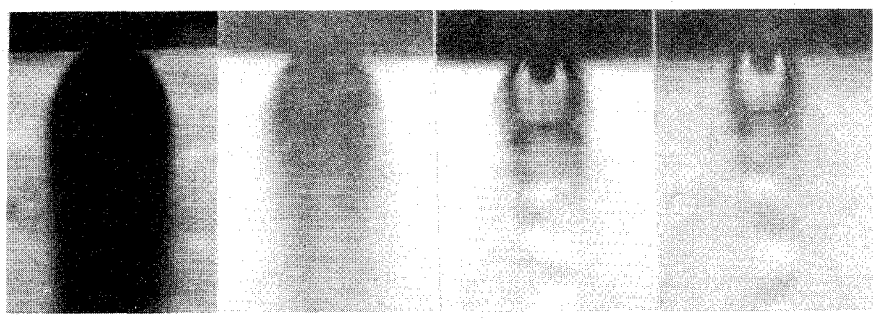

P_{inj}=5.8 MPa	P_{inj}=5.8 MPa	P_{inj}=5.8 MPa	P_{inj}=5.8 MPa
P_{chm}=0.14 MPa	P_{chm}=0.14 MPa	P_{chm}=0.14 MPa	P_{chm}=0.14 MPa
T_{inj}=293 K	T_{inj}=325 K	T_{inj}=338 K	T_{inj}=365 K

Fig. 9 Schlieren photographs of ethylene jets injected at various injection temperatures.

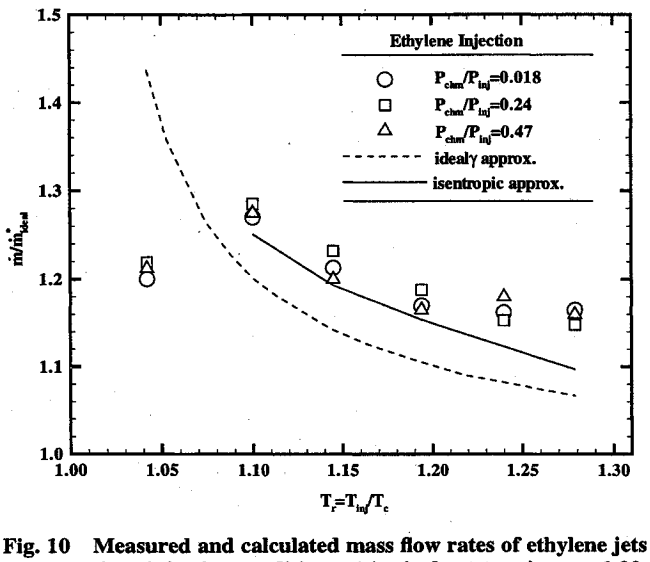

Fig. 10 Measured and calculated mass flow rates of ethylene jets under various injection conditions; $\dot{m}^*_{ideal}$ is the rate using $\gamma = 1.22$. The ideal γ approximation is calculated from Eq. (3) using γ under fuel injection conditions, while the isentropic approximation considers the near-critical-point thermodynamic properties.

Mass Flow Rate Measurements

Nozzle mass flow rates were measured using a Coriolis-type mass flow meter to characterize 1) the injection processes of supercritical ethylene and 2) the effects of near-critical-point thermodynamic properties on nozzle choking. Measured mass flow rates were normalized by a choked mass flow rate calculated assuming ideal-gas behavior and isentropic flow. The calculated results, referred to as ideal choked mass flow rates, were obtained by substituting a widely used mean specific heat ratio of 1.22 for ethylene at room temperature and atmospheric pressure[16] into Eqs. (1) and (2). The normalized choked mass flow rates would not be temperature dependent if the ethylene were an ideal gas with constant specific heats. Therefore, the normalization demonstrates the effects of near-critical-point thermodynamic properties on the ethylene injection process.

Figure 10 shows the normalized mass flow rates vs reduced injection temperatures of the fuel at P_{chm}/P_{inj} of 0.018, 0.24, and 0.47. Mass flow rates are constant and are insensitive to increases in chamber pressure when the flow is choked. This phenomenon was observed for the present case: the mass flow rates varied less than ±2% when P_{chm}/P_{inj} was increased from 0.018 to 0.47.

Ratios of measured and calculated ideal choking mass flow rates first increase as the thermodynamic critical temperature is approached and then decrease slightly at T_r = 1.04. The predicted mass flow rates are 10% lower at T_r = 1.28, and more than 25% lower at T_r = 1.10, indicating that the ideal-gas isentropic-flow approximation with a specific heat ratio of 1.22 can lead to significant error if it is applied to supercritical fuels. Smaller $\dot{m}/\dot{m}^*_{ideal}$ at higher temperatures indicates that supercritical fuel behaves more like an ideal gas as its thermodynamic state moves farther away from the critical point. This finding supports the conclusions drawn from the schlieren photographs (Fig. 9) for conditions of T_{inj} = 338 and 365 K.

Another approach to the ideal-gas isentropic-flow approximation was developed using the specific heat ratio under fuel injection conditions.[4] Results from this approximation are plotted as a dashed line in Fig. 8 and referred to as the ideal γ approximation. This approximation underpredicts the measured values by about 7% when $T_r \geq 1.10$, and overpredicts significantly at T_r = 1.04. The good agreement for $T_r \geq 1.10$, however, is fortuitous. Based on the assumption of an ideal gas, the increase in specific heat ratio leads to overprediction of the speed of sound, which compensates for the underprediction of fluid density, and yields the observed trend. This ideal γ approximation has two other major failures. First of all, it fails to predict the mass flow rate at T_r = 1.04, where different injection processes are involved. One possible explanation, which will be discussed later in the consideration of thermodynamic injection paths, is that liquid and gas phases coexist at the nozzle exit. Secondly, the ideal γ approximation predicts incorrect ratios of nozzle exit to injection choking pressures and temperatures. As T_r decreases from 1.29 to 1.04, the approximation yields choked ratios of fluid pressure at the nozzle exit to injection pressure $(P_e/P_{inj})^*$ from 0.517 to 0.290, and choked ratios of fluid temperature at nozzle exit to injection temperature $(T_e/T_{inj})^*$ from 0.810 to 0.393. These results imply that flow at the nozzle exit is subsonic for T_r = 1.04 and 1.10 when P_{chm}/P_{inj} = 0.47. This argument, however, contradicts the present observations because the mass flow rates with P_{chm}/P_{inj} = 0.018, 0.24, and 0.47 are the same within experimental uncertainties, indicating a choked and sonic condition.

To elucidate the injection process of supercritical ethylene, an isentropic-flow approximation considering near-critical-point thermodynamic properties was developed. This approximation does not require assumptions of constant specific heat ratios and ideal-gas state relations. The thermodynamic properties were calculated based on data from Younglove,[4] and an iterative procedure was used to calculate the choking mass flow rate. The entropy and enthalpy of the injection state were obtained, and an exit pressure was estimated. The fluid thermodynamic state at the nozzle exit was then determined based on the estimated pressure and the injection entropy; the fluid enthalpy and speed of sound at this state were then calculated. The exit velocity was derived from the one-dimensional energy equation, assuming negligible upstream velocity:

$$h_{inj} = h_e + u_e^2/2 \tag{4}$$

Table 2 Nozzle exit properties for choking conditions[3,4]

T_{inj}/T_c	$(Pe/P_{inj})^*$	$(Te/T_{inj})^*$	ρ_e, kg/m^3	μ_e, 10^{-7} Pa·s	a_e, m/s	$Re \times 10^{-6}$
1.100	0.572	0.878	61.1	113	253	1.38
1.145	0.572	0.876	53.2	109	271	1.33
1.194	0.572	0.880	47.6	116	287	1.18
1.240	0.570	0.884	43.6	119	299	1.11
1.279	0.569	0.892	40.5	122	310	1.03

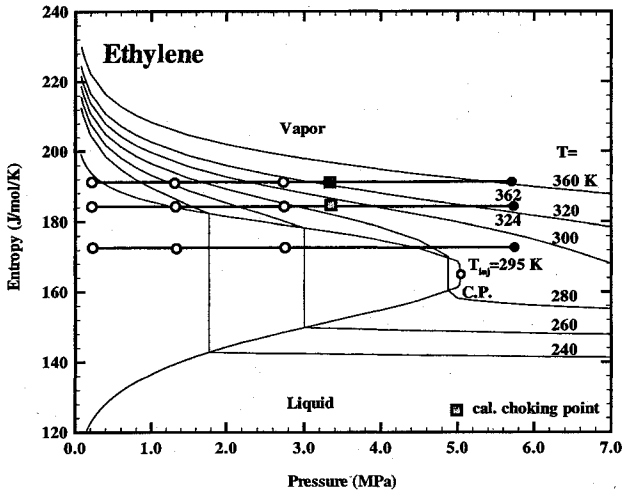

Fig. 11 Thermodynamic paths of injection processes within the nozzle at T_{inj} of 295, 324, and 362 K.

If the calculated exit velocity is lower than the speed of sound at the estimated pressure (as given by Younglove[4]), a subsonic jet should result. A lower pressure was then estimated, and the procedure was repeated. If the calculated exit velocity is larger than the speed of sound, a larger exit pressure was used to repeat the procedure. Linear interpolation was used for simplicity, and the iteration stopped when the exit velocity was within 0.5 m/s of the speed of sound. Calculated choking conditions are listed in Table 2. These mass flow rates were normalized with the values from the ideal-gas isentropic-flow approximation and plotted as a solid line in Fig. 10.

The isentropic-flow approximation, which considers the near-critical-point thermodynamic properties, yielded mass flow rate values that are very close to the measured values: about 2% less than the measured values at $T_r = 1.10-1.20$ and about 6% less at $T_r = 1.28$. The larger discrepancy at $T_r = 1.28$ may be attributed to the greater uncertainties in the injectant temperature at high temperatures because of the limitations of the heat exchanger. The calculated and measured values have the same trend; $\dot{m}/\dot{m}^*_{ideal}$ increases as T_r decreases. Isentropic analysis may explain this phenomenon. The fluid density increases from 40.5 to 61.1 kg/m^3 as T_{inj} decreases from 362 to 311 K. The fluid speed of sound, however, decreases from 310 to 253 m/s. Since the nozzle exit cross section was the same in each case, the increase in choked mass flow rate is attributed to the large increase in fluid density. With $T_r = 1.04$ and the assumption of an isentropic process, the final state is within the liquid–gas mixture regime. No calculation was made for this case.

Predicted choked pressure ratios $(P_e/P_{inj})^*$ and choked temperature ratios $(T_e/T_{inj})^*$ are also given in Table 2. $(P_e/P_{inj})^*$ decreases from 0.572 to 0.569, and $(T_e/T_{inj})^*$ increases from 0.878 to 0.892 as T_r increases from 1.100 to 1.279. These ratios approach the values of $(P_e/P_{inj})^* = 0.561$ and $(T_e/T_{inj})^* = 0.901$, which are predicted by the ideal-gas isentropic-flow approximation with a specific heat ratio of 1.22. The increase in $(P_e/P_{inj})^*$ and the decrease in $(T_e/T_{inj})^*$ as the critical temperature is approached are apparently because of the unusual near-critical-point thermodynamic properties of the injectant fluid; these ratios approach the ideal-gas values as the temperature is increased beyond the critical temperature.

Thermodynamic Paths of the Injection Processes Within the Nozzle

The injection processes of supercritical ethylene within the nozzle passage are illustrated on a thermodynamic chart of entropy vs pressure in Fig. 11. Selected isotherms corresponding to the present test conditions are identified, along with saturated liquid and vapor boundaries; C.P. denotes the critical point. Injection processes are assumed to be isentropic within the nozzle passage as indicated in the isentropic approximation, and to avoid confusion only three injection temperatures, 295, 325, and 362 K, were selected. Solid circles represent the initial injectant thermodynamic state, while open circles represent chamber pressures. Chamber pressures are the final pressures if the nozzle is not choked. If the nozzle is choked, the isentropic approximation is not valid outside the nozzle because of the underexpansion process and the normal shock wave (Mach disk). The square symbols denote the calculated onset choking pressure from the isentropic-flow approximation for the given injection pressure (see Table 2). Pressures lower than the onset pressures of the corresponding process indicate a choked condition.

At an injection temperature of 295 K, the constant-entropy line extends into the two-phase liquid–gas region; therefore, as indicated previously, the fluid may exist in two phases at the nozzle exit. The speed of sound of a water–air mixture in the dispersed phase varies with the void fraction and can be reduced to less than one-third of that of air at room temperature.[17] This may explain the observed lower mass flow rate at $T_r = 1.04$ (Fig. 8). As the injection temperature increases, fluid at the nozzle exit, as predicted assuming an isentropic process, is gaseous. The predicted choking pressure, about 3.3 MPa, indicates that the exiting flows are, in fact, choked. Additionally, the calculated choking points are in the gas state and away from the critical temperature. Therefore, the ethylene jets should exhibit shock structures similar to those of nitrogen jets, in agreement with the observations made with schlieren photography.

Conclusions

The injection of supercritical ethylene at conditions near the thermodynamic critical point was studied. The experimental apparatus was validated with nitrogen injection, and the results were used as a basis for comparison with supercritical ethylene injection. The major conclusions are as follows:

1) Near the nozzle exit, supercritical ethylene jets exhibited an opaque region which, in the most extreme case, persisted for a distance of more than 40 nozzle diameters. This opaque region, which is believed to be caused by fuel condensation, disappears as injection temperature increases. The length of the opaque region increases when the ambient pressure increases from atmospheric pressure to about 0.41 MPa, and then decreases if the ambient pressure is increased further.

2) At higher injection temperatures, the supercritical ethylene jets exhibited shock structures similar to those of a highly underexpanded ideal-gas jet. The supercritical ethylene jets generated a Mach disk, intercepting shock, and reflected shock at the nozzle exit. Locations of Mach disks were compared to values predicted for ideal gases. Good agreement was ob-

tained, which indicates that the Mach disk location is insensitive to fuel type. However, the shock structure of ethylene jets at lower injection temperatures is obscured by fuel condensation, and no definite conclusion can be drawn under these conditions.

3) Jet mass flow rates were found to increase as the injection temperature approached the thermodynamic critical value. For the present test conditions, mass flow rates were about 10–25% higher than the mass flow rates calculated with the ideal-gas isentropic-flow approximation using a specific heat ratio of 1.22. A second ideal-gas isentropic-flow approximation was developed using the specific heat ratio at the injection conditions. The approximation underpredicts the measured values slightly (about 7%) for most conditions, because of the large specific heat ratios near the critical point. This approximation, however, predicts incorrect ratios of nozzle exit to injection choking pressures and temperatures.

4) An isentropic-flow approximation, which takes into account the near-critical-point thermodynamic properties, was developed for ethylene, and the resulting predicted mass flow rates agree reasonably well with the measured values. This approximation produced the same trend of mass flow rates vs reduced temperature, indicating that the increased mass flow rate (at lower reduced temperatures) is caused by the large density increase (characteristic of fluid near its critical point).

5) Thermodynamic path analyses revealed that ethylene may pass through a liquid–gas regime at lower injection temperature. This suggests the possible coexistence of liquid and gas phases at the nozzle exit. At higher injection temperatures, calculated choking pressures were greater than the maximum ambient chamber pressure, in agreement with the observation that mass flow rates are insensitive to chamber pressures since the present injection conditions are choked.

Acknowledgments

This work was supported by and performed at U.S. Air Force Wright Laboratory, Wright–Patterson Air Force Base, OH under Air Force Contracts F33615-93-C-2300 and F33615-92-C-2022. The assistance of K. Kirkendall, G. Haines, D. Schommer, and C. Smith of Taitech, Inc., for apparatus development, and of A. E. S. Creese for editorial comments concerning this article are appreciated.

References

[1]Edwards, T., "USAF Supercritical Hydrocarbon Fuels Interests," AIAA Aerospace Sciences Meeting, AIAA Paper 93-0807, Reno, NV, Jan. 1993.

[2]Nieto de Castro, C. A., "Thermal Conductivity and Thermal Diffusivity in Supercritical Fluids," *Supercritical Fluid Technology: Reviews in Modern Theory and Applications*, edited by T. J. Bruno and J. F. Ely, CRC Press, Boca Raton, FL, 1991, Chap. 9.

[3]Holland, P. M., Eaton, B. E., and Hanley, H. J. M., "A Correlation of the Viscosity and Thermal Conductivity Data of Gaseous and Liquid Ethylene," *Journal of Physical and Chemical Reference Data*, Vol. 12, No. 4, 1983, pp. 917–932.

[4]Younglove, B. A., "Thermophysical Properties of Fluids: I. Argon, Ethylene, Parahydrogen, Nitrogen, Nitrogen Trifluoride, and Oxygen," *Journal of Physical and Chemical Reference Data*, Vol. 11, Suppl. 1, 1982, pp. 58–96.

[5]Faeth, G. M., "Structure and Atomization Properties of Dense Sprays," *22nd Symposium (International) on Combustion*, The Combustion Inst., Pittsburg, PA., 1990, pp. 1345–1352.

[6]Wu, P.-K., Tseng, L.-K., and Faeth, G. M., "Primary Breakup in Gas/Liquid Mixing Layers for Turbulent Liquids," *Atomization and Sprays*, Vol. 2, No. 3, 1992, pp. 295–317.

[7]Adamson, T. C., and Nicholls, J. A., "On the Structure of Jets from Highly Underexpanded Nozzles into Still Air," *Journal of Aerospace Sciences*, Vol. 26, No. 1, 1959, pp. 16–24.

[8]Crist, S., Sherman, P. M., and Glass, D. R., "Study of the Highly Underexpanded Sonic Jet," *AIAA Journal*, Vol. 4, No. 1, 1966, pp. 68–71.

[9]Chen, L. D., "Heat Transfer, Fouling, and Combustion of Supercritical Fuels," Univ. of Iowa, F49620-92-J-0462, Iowa City, IA, 1994, pp. 6–25.

[10]Hermanson, T. C., Papas, P., and Kay, I. W., "Structure and Penetration of a Transverse Fluid Jet Injected at Supercritical Pressure into Supersonic Flow," AIAA Paper 92-3652, July 1992.

[11]Yang, V., Hsieh, K. C., and Shuen, J. S., "Supercritical Droplet Combustion and Related Transport Phenomena," AIAA Paper 93-0812, Jan. 1993.

[12]Ramjee, V., and Hussian, A. K. M. F., "Influence of the Axisymmetric Contraction Ratio on Free-Stream Turbulence," *Journal of Fluids Engineering*, Vol. 108, Ser. I, No. 3, 1976, pp. 506–515.

[13]Shapiro, A. H., *The Dynamics and Thermodynamics of Compressible Fluid Flow*, Vol. I, Wiley, New York, 1953, pp. 73–105.

[14]Arnberg, B. T., "Review of Critical Flowmeters for Gas Flow Measurements," *Journal of Basic Engineering*, Vol. 84, Ser. D, No. 4, 1962, pp. 447–460.

[15]Szaniszlo, A. J., "Experimental and Analytical Sonic Nozzle Discharge Coefficients for Reynolds Numbers Up to 8×10^6," *Journal of Engineering for Power*, Vol. 97, Ser. A, No. 4, 1975, pp. 521–526.

[16]Baumeister, T., Avallone, E. A., and Baumeister, T., III, *Mark's Standard Handbook for Mechanical Engineers*, 8th ed., McGraw–Hill, New York, 1978, pp. 4–17.

[17]Wallis, G. B., *One-Dimensional Two-Phase Flow*, McGraw–Hill, New York, 1969.